JOURNAL OF RESEARCH of the National Bureau of Standards—A. Physics and Chemistry
Vol. 72A, No. 5, September–October 1968

Electron Impact Excitation of Hydrogen Lyman-α Radiation

Robert L. Long, Jr.,*† Donald M. Cox,* and Stephen J. Smith**

Joint Institute for Laboratory Astrophysics††

(May 8, 1968)

An experimental investigation of electron impact excitation of the $2p$ state of atomic hydrogen is described. A beam of electrons was passed through a chopped beam of hydrogen atoms in a high vacuum apparatus. The modulated flux of Lyman-α photons emitted in the radiative decay of the $2p$ state was taken as a measurement of the excitation probability resulting from direct excitation plus indirect excitation resulting from cascading. The region surrounding the intersection of the two beams was electrically and magnetically shielded to prevent quenching of metastable $2s$ atoms and thereby to ensure that the observed Lyman-α flux resulted from decay of the short-lived $2p$ state. The experimental results are consistent with those obtained by Fite, Stebbings, and Brackmann [1959], and confirm the existence of a large discrepancy between theoretical and experimental results in the electron energy range below 50 eV.

Key Words: Atomic hydrogen; beams; electron impact excitation; experimental; high vacuum; Lyman-α.

1. Introduction

The scattering of electrons by hydrogen atoms is the simplest atomic scattering process and therefore a convenient prototype of scattering problems for light atoms. In addition, it is an important astrophysical process, particularly in stellar atmospheres. For these reasons it has earned much theoretical and some experimental attention [Moiseiwitsch and Smith, 1968; Burke and Smith, 1962]. The number of experimental investigations has been restricted primarily due to the difficulty of producing atomic hydrogen but these investigations are necessary for critical evaluation of the theoretical calculations.

Inelastic collisions of electrons with ground state hydrogen atoms can produce excited atoms in the $2p$ state which quickly decay to the ground state with the emission of Lyman-α (1216 Å, 10.2 eV) radiation:

$$\mathrm{H}(2p) \rightarrow \mathrm{H}(1s) + \mathrm{Ly}\text{-}\alpha. \tag{1}$$

The primary process for production of H($2p$) is direct excitation:

$$e^- + \mathrm{H}(1s) \rightarrow e^- + \mathrm{H}(2p). \tag{2}$$

A significant number of atoms in the $2p$ state can also be produced by cascade processes:

$$e^- + \mathrm{H}(1s) \rightarrow e^- + \mathrm{H}(nl), \tag{3}$$

$$\mathrm{H}(nl) \rightarrow \mathrm{H}(2p) + h\nu, \tag{4}$$

where H(nl) represents any excited state that can spontaneously decay to the $2p$ state, by a direct or indirect route. The radiation $h\nu$ in eq (4), shown as a direct process, will be in a line of the Balmer series. An appreciable number of metastable $2s$ state hydrogen atoms are also produced by processes similar to those given in eqs (2), (3), and (4). The shape of the cross section for metastable production has been measured [Lichten and Schultz, 1959; Stebbings, Fite, Hummer and Brackmann, 1961; Hils, Kleinpoppen and Koschmieder, 1966]. Born approximation calculations suggest that the peak value of the $2s$ state excitation cross section is about one-fifth of that for the $2p$ state.

Measurements of the relative amount of Lyman-α radiation emitted in the decay of the H($2p$) atoms produced by electron collisions have been made [Fite and Brackmann, 1958; Fite, Stebbings and Brackmann, 1959; Chamberlain, Smith and Heddle, 1964; Williams, Curley and McGowan, 1968] primarily in order to obtain information about the cross section for the direct excitation of H($2p$), as given in eq (2). A difficulty arises in the interpretation of the measure-

*Supported by NSF Grant No. 5959.
†Current Address: Sandia Laboratory, Albuquerque, N.M. 87115.
**Staff Member, Laboratory Astrophysics Division, National Bureau of Standards, and the University of Colorado Campus, Boulder, Colorado 80302.
††Of the National Bureau of Standards and University of Colorado.

ments because of the cascade processes (eqs (3)-(4)) that also yield H($2p$) atoms. However, the situation is fairly simple in two energy regions:

1. At energies below the threshold for excitation of the $n=3$ states of hydrogen (12.1 eV), no cascade processes can occur and the excitation of the H($2p$) state can be observed directly.

2. At electron energies greater than 100 eV, Born approximation calculations of electron-hydrogen atom excitation are believed [Silverman and Lassettre, 1966] to be reasonably accurate and cascade corrections can be estimated. Furthermore, the calculated cascade contribution [Moiseiwitsch and Smith, 1968] is only about 2 percent of the total Lyman-α radiation for electron energies in the neighborhood of 200 eV. The intermediate range of 12.1 to 100 eV is complicated by larger cascade components.

The first measurements of the electron impact excitation of Lyman-α photons emitted from the $2p$ state of atomic hydrogen were carried out by Fite and his collaborators [Fite and Brackmann, 1958; Fite et al., 1959]. Using a modulated crossed beam technique and observing the Lyman-α photons resulting from excitation in a field free region, to avoid quenching of $2s$ atoms, they obtained a relative cross section, including cascading, with confidence limits stated as being about ± 12 percent. These measurements, even with the relatively large assigned errors, have played a very important role because they depart quite significantly from theoretical results for direct $2p$ state excitation in the energy range below about 70 eV. It is not possible to explain the departures in terms of cascading.

A series of elaborate close coupling calculations was undertaken [Burke, 1963; Burke, Schey, and Smith, 1963] by P. G. Burke and his associates with limited success at narrowing the gap between theory and experiment. The difference remains very large in the first 20 v above threshold.

This paper describes a program undertaken with the objectives of verifying and improving on the H($2p$) excitation measurements of Fite et al. The work described here is the development of measurement technology and the effort to improve that technology to the point that results accurate to within a few percent might be made available for a critical test of the ability of theory to accurately predict properties of the simplest atom.

A detailed description of the apparatus is presented in section 2. This is followed by an outline of the procedures for data acquisition and reduction in section 3. Some results and a discussion of accuracy are given in section 4. Discussion of the current experimental data and some of the theoretical calculations appear in section 5.

2. Experimental Apparatus

The measurement used the high-vacuum crossed beam method, shown schematically in figure 1, involving a chopped atomic beam (D) of hydrogen

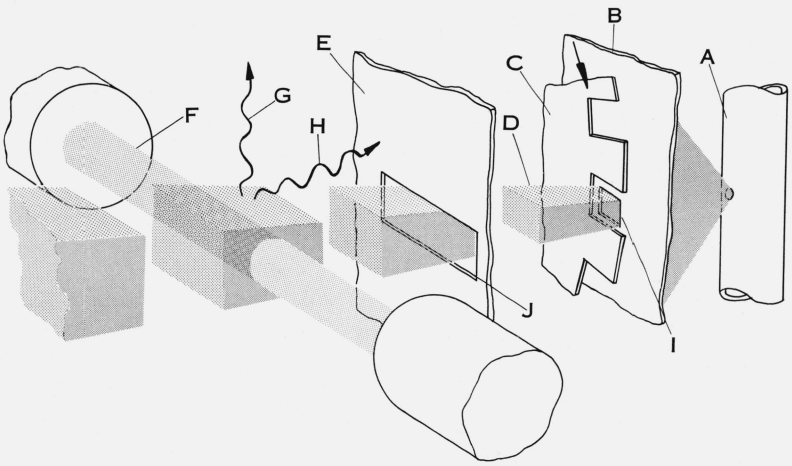

FIGURE 1. *Schematic diagram of the crossed beam configuration.*

A—the 4.8 *mm* I.D. tungsten dissociator with a 0.8 *mm* hole to permit the emission of gas; B—the bulkhead to the source chamber, which mounts the 2.5 *mm* × 2.5 *mm* field aperature (I) at a distance of 4.6 *cm* from the source, to define the atom beam (D); C—the chopping wheel consisting of twenty teeth on a wheel rotated at 5 revolutions per second; E—the bulkhead to the buffer chamber, with a differential pumping aperature (J) which plays no part in defining the atom beam; F—the electron beam which intersects the chopped atom beam at a point 9.5 *cm* from the source, to excite photons which are detected by means of ionization chambers placed to intercept emission in particular directions (G and H) perpendicular to the atom beam axis.

gas which was intersected at right angles by an electron beam (F). A fraction of the Lyman-α photons which were emitted in a particular direction, such as perpendicular (G) to the plane containing the electron and hydrogen beams was detected in an ionization chamber. The relative Lyman-α production cross section, $Q_\perp$, was given by

$$Q_\perp = (S - S_0)/IP, \tag{5}$$

where S is proportional to the ion chamber current during Lyman-α production, S_0 is proportional to the apparent ion chamber current without Lyman-α production, I is the total electron current, and P is a pressure proportional to the hydrogen atom beam intensity.

2.1. Vacuum System

The apparatus was a fairly conventional atomic beams machine (see fig. 2). The vacuum chamber was divided into three compartments (by bulkheads as shown in fig. 1 and fig. 2b): a source chamber, which was pumped by a 70 liter/sec (l/s) diffusion pump and by a titanium sublimator; a buffer chamber, also pumped by a 70 l/s diffusion pump; and an interaction chamber, which was pumped by a 600 l/s diffusion pump. Mercury, instead of oil, diffusion pumps were chosen to minimize potential sources of background hydrogen gas and to avoid possible deposition of undesirable insulating films on the electron gun structure. A water-cooled baffle and a liquid nitrogen-cooled trap were used above each diffusion pump to prevent mercury vapor from entering the system. A sorbent trap was installed in the foreline to catch organic vapors from the forepump. Welded stainless steel construction was used wherever feasible and connections were made with metal gaskets. These measures enabled low pressure, less than 4×10^{-8} torr (nitrogen equivalent), to be maintained in the interaction chamber with pressures of about 1×10^{-7} and 1×10^{-6} torr in the intermediate and source chambers, respectively, while hydrogen gas was flowing into the system. The base pressure in the interaction region was as low as 1 or 2×10^{-8} torr. No baking of the chamber was employed except for mild outgassing of the titanium deposition surface.

2.2. Atomic Beam

The hydrogen atoms were produced by thermal dissociation of molecular hydrogen gas. This method is preferable to some others, e.g., radio frequency discharge dissociation, because no excited atoms are produced. Also under the assumption of thermal

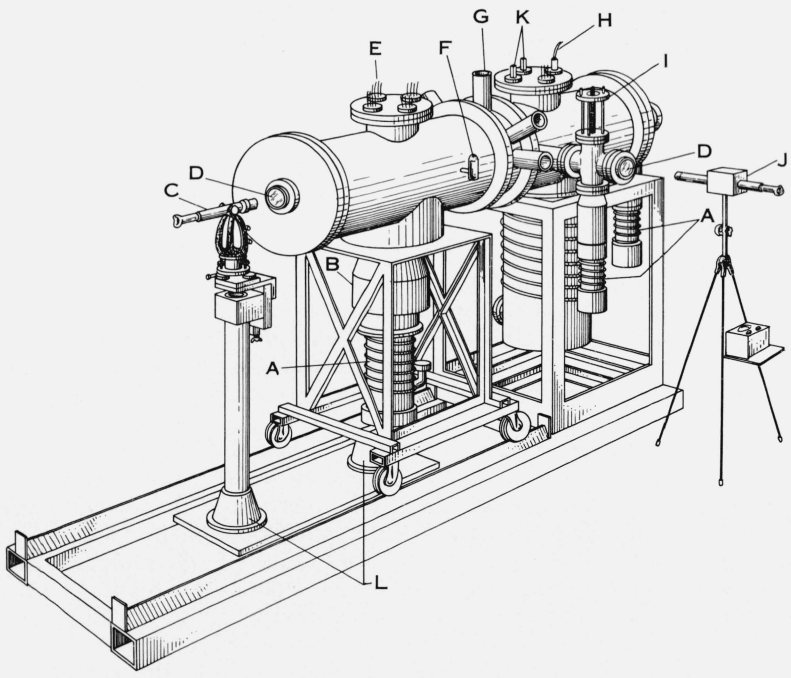

FIGURE 2a. *Hydrogen beam apparatus.*

A—mercury vapor diffusion pumps; B—liquid nitrogen cooled trap; C—alignment telescope (on the hydrogen beam axis); D—windows; E—electrical feed throughs; F—ionization type vacuum gauge (three vacuum gauges are utilized: one as shown, one for the hydrogen source chamber and one for the chopper chamber); G—shielded electrical feedthroughs for the Lyman-α detectors and electron gun current measurement; H—hydrogen gas inlet; I—valve for mercury diffusion pump; J—optical pyrometer (views the furnace); K—heavy copper feedthroughs for furnace power; L—fixed base for alignment telescope.

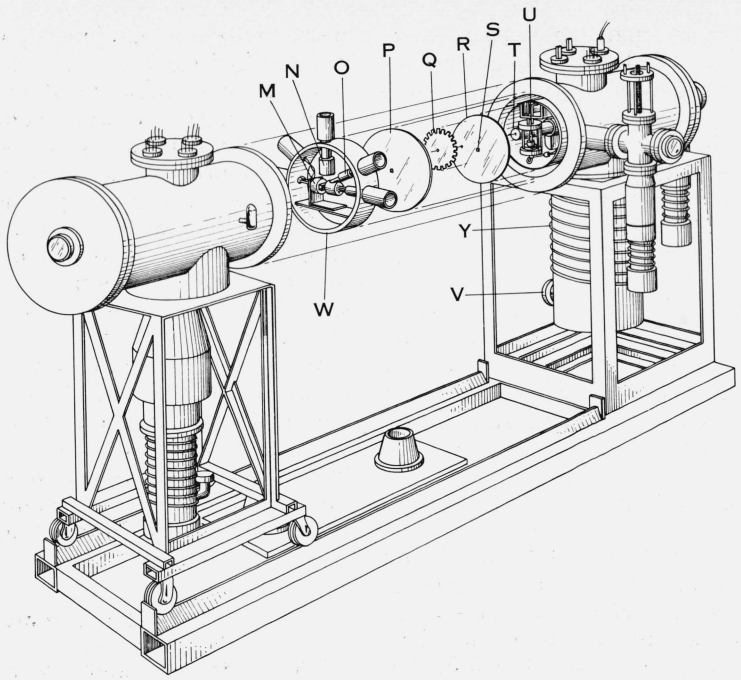

FIGURE 2b. *Hydrogen beam apparatus (expanded view).*

M—electron gun; N—Lyman-α photon detector positioned at ninety degrees with respect to the electron beam; O—Lyman-α photon detector positioned at thirty degrees with respect to the electron beam; P—partition to separate chopper (buffer) chamber and interaction chamber ("second partition"); Q—Chopper wheel; R—partition to separate chopper chamber and hydrogen source chamber ("first partition"); S—collimating slit for hydrogen beam ("field aperture"); T—chopper wheel driveshaft (a synchronous motor and gear train mounted outside the vacuum chamber is magnetically coupled through the rear flange to drive the chopper); U—tungsten furnace and support structure; V—header for titanium sublimation pump; W—removable stainless steel ring which supports the Lyman-α detectors and electron gun (the mechanism for positioning the ring is not shown; soft aluminum gaskets cut from sheet stock are used between knife edges machined on the ring and the main system to effect a vacuum seal); Y—casing for titanium sublimation pump.

equilibrium, an estimate of the absolute atomic beam intensity is possible. The gas was introduced into a glass plenum through a silver-palladium alloy leak [Hunter, 1960; Young, 1963] in order to purify the ordidary tank hydrogen gas used and was piped into a tubular tungsten furnace. The furnace tube was made from tungsten foil, 0.013 mm thick, rolled up on a mandrel, 4.8 mm in diam, four layers thick. A hole, 0.8 mm in diameter, was drilled through the wall of the tube at its center, allowing the gas to flow out into the source chamber.

In order to dissociate hydrogen, the tungsten furnace was resistance heated to about 2500 K with a direct current of approximately 125 A (about 425 W of power was required including line losses). The temperature was measured with an estimated accuracy of ± 15 K by means of an optical pyrometer which viewed the side of the furnace near the exit hole. Corrections for the emissivity of tungsten [Kohl, 1960; Poland, Green and Margrave, 1961] and window transmission [Foote, Fairchild and Harrison, 1921] were applied. The furnace pressure was estimated from measurements of the molecular hydrogen pressure at the plenum near the silver-palladium leak (a calibrated high pressure ion gauge was used) and the conductances of the tubulation leading to the furnace and of the furnace exit.

The lateral dimensions of the atomic beam were determined by the square (2.5 mm × 2.5 mm) field aperture in the first bulkhead (see figs. 1 and 2b). The aperture in the second partition did not collimate the atomic beam but served to reduce the gas flow into the interaction chamber from the background gas in the volume surrounding the furnace. With a furnace temperature of 2500 K and a typical furnace pressure of 25 millitorr, the calculated atomic beam intensity passing through the field aperture, assuming effusive molecular flow from the furnace, was 9.85×10^{13} atoms sec^{-1}. The atomic beam cross section of uniform density at 9.5 cm from the furnace exit, where the electron beam axis intersects the atomic beam axis, was 4.6 mm × 4.6 mm; and the average atom density there in a fully dissociated beam would be 2.2×10^{8} atoms cm^{-3}.

2.3. Chopper

The atomic beam chopper was located in the intermediate chamber of the vacuum system. The chopper was a toothed wheel which was rotated by a synchronous electric motor so that the teeth interrupted the beam 100 times per second with a duty cycle of 0.5. This enabled the use of a narrow band, a-c amplifier for the photon signal. The detection bandwidth was further reduced by using synchronous demodulation of the a-c signal. The reference signal was derived from a photocell that viewed a beam of light which also was interrupted by the atomic beam chopper. Such a-c techniques have the advantage of greater gain stability than would be possible with a d-c amplifier: lower electronic noise than a wide band amplifier, and elimination of the undesired, unmodulated photon signals produced in collisions of electrons with the hydrogen background gas or the electron gun electrodes.

2.4. Electron Gun Structure

A cross sectional diagram of the electron gun, Faraday cage, and retarding potential analyzer is shown in figure 3. The source of electrons was an indirectly heated, impregnated cathode (Phillips type BP-1B),[1] electrode W. It acted as the first element of a Soa-type acceleration stage [Simpson, 1961] which also included the grid, electrode F, and the anode, electrode G. This stage was followed by a lens consisting of a second plate at anode potential, electrode H, and the grounded electrode I which focused the electrons into the Faraday cage (electrodes L and M). This lens was operated as a decelerating lens for cathode potentials $\leqq 90$ V, where the anode-cathode potential difference was not inconveniently large, and as an accelerating lens for cathode potentials $\geqq 70$ V. The overlap at 70 to 90 V in these two modes was used to test whether results were independent of focusing mode; gross disagreement occasionally observed between the two modes could be eliminated by cleaning the gun electrodes and was evidently due to surface charging effects. The cathode holder was made of stainless steel, electrodes F and G were molybdenum, and the remaining electrodes were gold plated Advance or stainless steel.

The electron beam axis intersected the atomic beam axis in the interaction region between electrodes J and K. The interaction region was enclosed by gold plated nickel mesh, approximately 85 percent transparent, supported by a rectangular framework fastened to the grounded electrode J. The mesh provided shielding against electric fields from the high voltage leads to the ion chamber and the electron gun, thereby preventing disturbance of the electron beam and electric quenching of the metastable hydrogen atoms in the $2s$ state. The quenching, which can be significant for fields as low as 1 V cm^{-1} [Luders, 1950], would result in Lyman-α photons indistinguishable from those produced by excitation of the $2p$ state. Maximum space charge fields were a few tenths of a volt per centimeter at threshold for currents used (see fig. 4) assuming a 1 mm beam radius at the interaction region. These fields would reduce the mean life from 1/7 s in field free space to about 10^{-2} s. The atoms spend less than 10^{-4} s in the interaction region. Magnetic field quenching of the metastable atoms was prevented by a magnetic shield installed around the electron gun structure, which gave a residual field of less than 10 mG. Thus the metastable atoms drifted out of sight of the photon detector before decaying.

The apertures in electrodes H through J were 2.4 mm in diameter to ensure that all of the electron beam passed through the umbra of the larger atomic beam and that it then entered the Faraday cage. A guard electrode (K) with an aperture 4 mm in diameter was mounted in front of the Faraday cage (aperture 5 mm) to detect any excessive spread in the electron beam diameter. The electron beam focus, controlled by the potential difference between the anode and cathode of the electron gun for each cathode potential, was selected by obtaining near minimum guard electrode current and near maximum Faraday cage current. The potential of the grid controlled the magnitude of the total current and was 1–3 V positive with respect to the cathode, depending on the amount of current desired. For currents less than 10 μA, the guard current was less than 0.3 percent of the Faraday cage current at cathode potentials greater than 14 V. It was at most one or two percent of the Faraday cage current at 9 eV, but was critically dependent on the primary current. Evidently the effect at low energy is a space charge limitation. All currents were measured with low impedance meters, so that the electrodes were less than 8 mV from ground potential, in order to minimize stray electric fields.

Approximate calculations of the focusing properties of the electron gun showed that the focus of the electron beam occurred inside the Faraday cage for both focusing modes. These calculations also indicated that the electron path length through the hydrogen beam for the extreme electron trajectories differed by no more than 1/4 percent from a path parallel to the axis for the two focusing modes. Any larger disagreement between signals from the two different focusing modes for the same electron energy should therefore be caused by some other effect.

The Faraday cage which was used to collect the electron current was composed of electrodes L and M and the electrodes immediately beyond them. No magnetic field was used to collimate the electron beam so the reflection of the incident electrons from the rear of the cage is assumed to be approximately diffuse. The probability of reflected and secondary electrons escaping from the cage was small because the solid angle subtended by the entrance aperture at the rear of the cage was only about 0.01 sr. There-

[1] Certain commercial materials are identified in this paper in order to adequately specify the experimental procedure. In no case does such identification imply recommendation or endorsement by the National Bureau of Standards, nor does it imply that the material identified is necessarily the best available for the purpose.

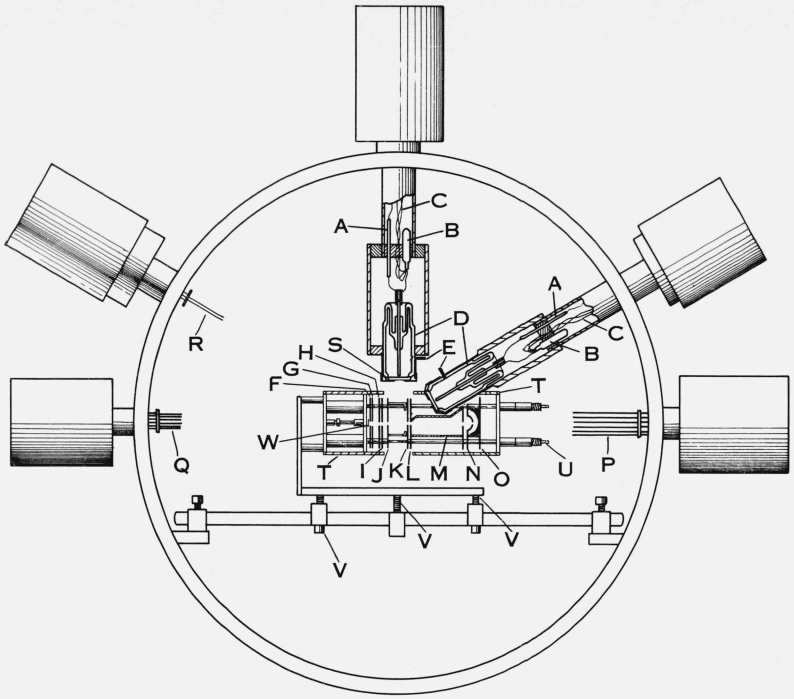

FIGURE 3. *Cross-sectional view in the plane of the electron beam axis and perpendicular to the atom beam axis.*

The inside diameter of the ring is 16 in. A, B, and C show elements of the input stages of the low noise preamplifiers sealed into bulkheads near the ionization chambers (D) for minimum stray input capacitance. The grid of the input tube (B) is operated near ground potential with d-c feedback through a 10^{10} Ω resistor (A). The ion chamber voltage (~ -550 *V*) is applied to a cylindrical electrode consisting of a platinized layer on the inside of the glass shell connecting to leads E. The electron gun, consisting of cathode W and electrodes F through O, is discussed in the text (Section 2.4). Leads in the multiple feed-through P are connected to electrodes K, L–M–N, and O for current measurements using high impedance electrometers. Feedthrough Q is used for applying electron gun and ionization chamber voltages. Feedthrough R is used for the gun cathode heater, S identifies a MgF_2 window which provides the short wavelength cut-off of the detector. T identifies magnetic shields, U the steel rods on which the gun is assembled using glass tubing as insulators and spacers, and V the leveling screws used to align the gun.

fore the current collection efficiency of the cage was high for all electron energies used.

The eccentric shape of the cylindrical part of the Faraday cage was provided to allow mounting of an ion chamber at an angle of 30° from the axis of the electron beam. This detector, installed in addition to the one at 90°, is intended for use in measurements of the angular distribution of Lyman-α photons. Sectors were cut out of both electrodes K and L to allow this chamber to view the interaction region. In order to prevent consequent stray electric fields in that region, wire mesh was fastened across the aperture in electrode L.

The rear electrode of the Faraday cage had a hole 1 mm in diameter at its center which allowed a small percentage of the electron current to pass into the hemispherical retarding potential analyzer [Simpson, 1961]. This analyzer was composed of electrodes N and O (see fig. 3) and had a design resolution, $\Delta E/E$, of 0.25 percent. The energy distribution could be measured at any cathode voltage by a modulated retarding potential technique [Leder and Simpson, 1958]. The full energy width at half maximum of the distribution was 0.3 to 0.5 eV, depending on the state of the cathode. The energy of the peak of the measured distribution (i.e., the most probable electron energy) was taken to be the effective electron beam energy in the interaction region. This assumption led to values for the threshold energy for production of Lyman-α photons within 0.15 eV of the spectroscopic value (10.2 eV). The retarding potential at which the peak occurred was about 1.5 V lower than the applied cathode potential; this difference was attributed to contact potentials. The instantaneous value of the contact potential depended upon the previous history of the system and whether or not hydrogen gas was flowing but it varied less than 50 mV during a day, after equilibrium with flowing hydrogen was achieved. Data taken on different days, with identical applied voltages, may have had somewhat different

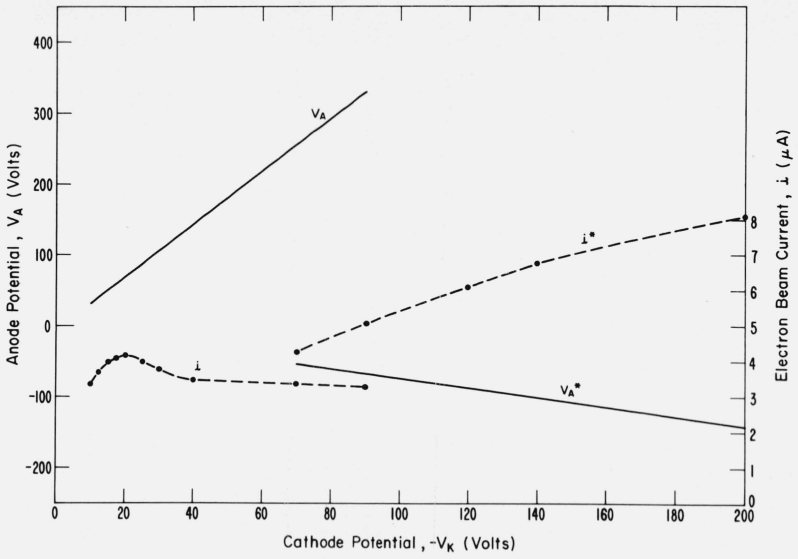

FIGURE 4. *Typical values of anode potentials* (V_A), *relative to laboratory ground, as a function of negative cathode potential* ($-V_K$).

The electron gun anode was programmed to these voltages in order to maintain desired focal properties as the electron beam energy was changed. Corresponding electron currents were those observed in taking the data summarized in table 2. The unstarred values are in the decelerating lens mode and starred values are in the accelerating lens mode (see text, sec. 2.4).

average contact potentials. The energy scale accuracy is estimated to be about ± 0.2 eV. The calibration of the cathode voltage power supply was checked by a digital voltmeter and did not change more than 0.15 percent. The electron energies for the data presented in section 4.2. were corrected both for the average contact potential and for deviation of the cathode power supply from the nominal, programed voltage.

All measurements of the total electron beam current were made with the two retarding potential electrodes connected to the Faraday cage current meter. The best gun operation was obtained for electron beam currents less than 10 μA but currents larger than 30 μA could be obtained, especially at the higher cathode potentials. In figure 4 are shown electron gun operating voltages and current yields typically used in a measurement.

2.5. Lyman-α Detector

Photons produced at the junction of the electron and hydrogen atom beams were detected by an ion chamber located on an axis perpendicular to the plane containing the crossed beams. The entrance aperture to the ion chamber was limited by a metal cap with an opening 6.9 mm $\times$ 19 mm, the longer dimension being perpendicular to the electron beam axis. Wire mesh about 85 percent transparent was stretched across this opening for electric shielding. Since this cap was 32 mm from the electron beam axis and its opening was centered on the intersection of the beams, photons from the center of the interaction volume could enter the ion chamber if they came off at 84° to 96° away from the electron beam axis within an azimuthal range of 33°. (The threshold data presented in sec. 4.1. were taken with the face of the detector mounted 16 mm from the interaction volume center. Therefore, the angles were larger in that experiment.) Metal strips were fastened to the top of the interaction region enclosure to leave an opening there of the same size as, and centered on, the opening in the ion chamber. These shields reduced the possibility of detecting photons emanating from regions other than the junction of the atom and electron beams, especially reflected photons, thereby preserving the angular resolution of the measurement and minimizing the background.

The front window of the ion chamber was required to transmit the 1216 Å Lyman-α radiation. Originally cleaved LiF (1.5 mm thick) was used but later (see sec. 4.2) polished MgF_2 (1 mm thick) was used. Both materials were obtained from the Harshaw Chemical Company. Care was taken to select pieces expected to have transmissions least dependent on light polarization, since the polarization of the Lyman-α radiation changes with electron energy [Percival and Seaton, 1958; Ott, Kauppila, and Fite, 1967]. The window had a clear diameter of about 16 mm and was cemented to the glass body of the ion chamber with low vapor pressure epoxy cement. The inner surface of the body was platinized to provide the negative electrode. The central tube (see fig. 3) was the electron current collector. A grounded Kovar ring was installed interrupt-

ing the glass envelope between the two electrodes in order to reduce leakage current to the center electrode, which was operated at very high impedence near ground potential.

The ionizing gas used in the ion chamber was nitric oxide, which has an ionization threshold of 1340 Å [Carver and Mitchell, 1964]. Since the cutoff wavelength of the LiF (or MgF_2) window was at 1050 Å (or 1130 Å), [Heath and Sacher, 1966], this provided a detector which was sensitive over only a 290 Å (or 210 Å) band approximately centered on the wavelength of interest. Therefore, the ion chamber was insensitive to the radiation of all atomic hydrogen lines except Lyman-α. However, some of the radiation produced by excitation of the small fraction of H_2 molecules in the atomic beam was within the bandwidth of the detector; the amount of this contribution was calculated from data taken with a pure molecular beam, as described in section 3, and could be subtracted from the atomic plus molecular data.

In order to fill the ion chamber with pure nitric oxide gas, it was connected to a gas handling system through its central tube and pumped out by an oil diffusion pump having a liquid nitrogen-cooled trap. Prior to filling the chamber, a pressure of less than 8×10^{-8} torr was indicated by an ion gage in the gas handling system. Then the diffusion pump was valved off and nitric oxide gas was introduced into the chamber to a pressure of 15 ± 1 torr, as indicated by a mercury manometer trapped by a slush of ethyl alcohol and liquid nitrogen. After initial testing of the ion chamber with ultraviolet light from a hydrogen rf discharge lamp, the copper filling tube was pinched off to seal and disconnect it from the gas handling system. Further testing was done after it was installed in the apparatus.

The ion chamber was operated in the proportional counter mode. The gas gain, given by the ratio of the ion current with the body electrode at -550 V to that at -50 to -150 V (the latter range was roughly a plateau, cf. Carver and Mitchell [1964] fig. 5), was about 65. The photon intensity was measured relatively by monitoring the ion current in the chamber with an electrometer tube preamplifier [Smith and Branscomb, 1960] having an effective input impedance of 10^8 Ω and a voltage gain of about 30. The first stage tube and the grid resistor of the preamplifier were mounted inside the vacuum system in order to minimize the input capacitance so that the gain at 100 Hz, the frequency at which the atomic beam was chopped, would be maximized. The a-c output of the preamplifier was further amplified and then synchronously demodulated (cf. sec. 2.3).

Typical operating parameters for the ion chamber are indicated in the following estimate of the magnitude of the output current. Earlier measurements [Fite and Brackmann 1958; Fite et al., 1959] of the Lyman-α production cross-section shape gave $Q_\perp = 0.8\pi a_0^2$ near the peak, when normalized to the Born approximation at high energy. From dimensions given above, the entrance aperture of the ion chamber subtends a solid angle (Ω) of 0.13 sr and the effective electron path length (d) in the atomic beam is 0.54 cm. Using the atomic beam density (n_a) of 2.2×10^8 cm^{-3} given in section 2.2., an electron current (I) of 5μA, and assuming isotropic radiation, the photon intensity incident on the detector is

$$S = n_a d \frac{I}{e} Q_\perp \Omega/4\pi = 2.6\times10^3 \text{ photons sec}^{-1}$$

where e is the electronic charge. The transmission of the LiF window for Lyman-α photons [Heath and Sacher, 1966] is about 0.69 (about 0.65 for the MgF_2 window) and of the wire mesh in front of it is 0.85. The fraction of transmitted photons absorbed in the 2 cm active length of nitric oxide gas at 15 torr is 0.91, using the measured value of 65.4 cm^{-1} for the absorption coefficient [Watanabe, Matsunaga, and Sakai, 1967]. Taking the photoionization yield of nitric oxide at Lyman-α to be 0.81 [Watanabe, et al., 1967] and the gas gain of 65, the ion chamber current for the above photon intensity would be 1.1×10^{-14} A. The output of the preamplifier for this input current would be 34 μV, which could be readily amplified to the level required for measurement.

2.6. Alinement

In order to obtain a well defined atomic beam and ensure that the electron beam axis crossed it at the proper location, careful alinement of the apparatus was necessary. A jig transit was positioned with its optical alinement axis centered on the field aperture in the first partition (see fig. 2) and approximately parallel to the axis of the vacuum chamber. This partition was then removed and the furnace tube was installed with the exit hole centered on the alinement axis. The furnace position could be maintained by means of a vertical screw drive to within 0.25 mm in order to compensate for thermal motions. The first partition was then replaced, the transit alinement was readjusted if necessary, the atomic beam chopper and the second partition were installed, and the second aperture was centered on the alinement axis. The ion chamber was alined with machinist's gages to an axis through the mechanical center of the ring assembly. The ring was then positioned and clamped on the fixed part of the vacuum chamber with the ion chamber axis vertical so that the center of the ring coincided with the alinement axis. The electron gun axis was alined by means of its support screws to be level, and to intersect the alinement (i.e., atomic beam) axis and the center line of the ion chamber. The accuracy of the intersection of these three axes is estimated to be within 0.25 mm. The accuracy of the 90° angle between the electron beam and the ion chamber axis is estimated to be within 0.5°. Some movement of the electron gun was noticed when the gun cathode was heated but this was minimized by a clamp on the end of the gun structure and could be compensated by moving the furnace tube in the opposite direction.

3. Data Acquisition and Reduction

A demodulated photon signal, obtained as described in sections 2.3 and 2.5, is noisy due to statistical fluctuations (shot-noise) in the small photon flux and due to electrical noise from the amplifiers. The electrical noise is predominately due to sources in the preamplifier grid circuit [see Smith and Branscomb, 1960]. The most important of these are thermal noise in the 10^{10} Ω input resistor, shunted by 5 to 10 pF of stray and grid capacitance, and shot noise in the grid current of the first preamplifier tube. These two sources are comparable and are roughly equivalent to a noise current of a few times 10^{-16} A in a 1/10 Hz bandwidth. As a first step in reducing the effects of noise, the photon signal (S) was integrated for 10 s by an operational amplifier with a capacitor feedback element and the integrated voltage, $\int S dt$, was recorded. The Faraday cage current (I) was integrated simultaneously, although drift was usually negligible during a measurement. After recording these data at one cathode potential, the automatic programer which was used to set the electron gun voltages advanced to its next position. Following a delay of about 10 s to ensure electron beam equilibrium, the next integration was started. The sequence of preselected cathode voltages could be repeated as many times (typically 60 in 1 day) as desired. This frequent repetition of short observations was used to eliminate the effects of any possible long term drifts.

The integrated data, together with elapsed time, furnace temperature, cathode potential, and other information, were recorded automatically by a data acquisition system on punched paper tape. The punched paper tape was later used to generate punched cards which were convenient for manual editing of the data before reducing them with a digital computer.

In order to determine the baseline for the relative photon intensity measurements, data were taken during each cathode voltage sequence at an electron energy of about 8.5 eV, which was too low to produce photons with energy sufficient to ionize the nitric oxide in the ion chamber. Scatter in the baseline data, from electronic noise, was comparable to that which occurred in the Lyman-α signals at the higher energies. The average of all the integrated signals taken at 8.5 eV, $\int S_0 dt$, was designated the zero signal level and was subtracted from all the integrated photon signals to give values which were directly proportional to the Lyman-α photon intensity. If the 8.5 eV data appeared to have a significant time dependence, such as may arise from drift in the demodulator bias, they could be fitted to a straight line by the least squares method and a time dependent zero correction could then be made. The magnitude of the signal integral was checked periodically with the low level a-c preamplifier disconnected. This essentially noise-free signal always agreed with the average obtained for $\int S_0 dt$ within statistical errors.

The linearity of the current meter was checked using a Keithley model 261 picoampere source and corrections to the integrated current values were made, if necessary, by adding (or subtracting) a value (which always corresponded to the integral of less than 0.03 μA) to each current integral. Since this correction was effectively a zero correction, it could be represented by the term $\int I_0 dt$ which was defined above. This gave integrated current values which were linear within 0.5 percent over the range of measurements.

The data acquisition system was zeroed and calibrated before taking data each day; when checked after taking data, no significant changes were detected. Parameters that were monitored periodically during the day were the feedback voltage of the battery powered ion chamber preamplifier, the zero setting and emission current of the hydrogen gas plenum pressure gage circuit, the electron beam energy distribution, the electron gun contact potential, the zero level of the electron current integral, the photon signal demodulator output bias, the furnace temperature, and the positions of the furnace and electron gun.

The relative cross section, $Q_\perp$, for production of Lyman-α photons (including possible radiation from the small H_2 molecular component of the atomic beam) emitted perpendicular to the electron beam was given by the formula

$$Q_\perp(\mathrm{H}+\mathrm{H}_2) = \{\int S dt - \int S_0 dt\}/P_p\{\int I dt - \int I_0 dt\}$$

$$= \int S dt/P_p\{\int I dt - \int I_0 dt\} - \int S_0 dt/P_p\{\int I dt - \int I_0 dt\}. \quad (6)$$

Here P_p is the average plenum pressure (in millitorr) indicated by the gas manifold gage (held constant to within ±1 percent by adjusting the temperature of the silver-palladium leak). The other symbols were defined above. The ratios in eq (6) were computed from the data of each ten second integration and the individual relative values of $Q_\perp$ were calculated. All those values of $Q_\perp$ for the same electron energy (i.e., gun cathode potential) taken in one day then were averaged together. The standard deviation of each resulting average $Q_\perp$ was given by the square root of the sum of the squares of the statistical standard deviations of the two averaged ratios in eq (6), which were computed in the usual manner [Beers, 1957].

The contribution of the molecular component of the atomic beam was estimated from data taken with the furnace at several temperatures too low to produce dissociation, i.e., with a 100 percent molecular beam. Data were taken above 1000 K for comparison with those taken at room temperature. The two results were consistent in shape and magnitude when corrections for the pressure and temperature differences were made. The molecular contribution correction to be applied for each electron energy was calculated by use of the formula

$$\int S_M(T) dt = \left\{\int S_M(T_r) dt - \int S_M(T_r)_0 dt\right\}$$

$$\{(1-\gamma) n_F(T)/n_F(T_r)\}$$

$$\cdot \{\overline{v_M(T)}/\overline{v_M(T_r)}\} \cdot \{\overline{v'_M(T_r)}/\overline{v'_M(T)}\}. \quad (7)$$

Here T is the temperature of the furnace used in the measuring of the quantities in eq (7), $S_M(T)$ is the estimated photon signal due to H_2 molecules with the furnace at absolute temperature T, $S_M(T_r)$ is the average photon signal measured at a given electron energy with the furnace at room temperature $T_r(\cong 295$ K), $S_M(T_r)_0$ is the corresponding zero correction, $n_F(T)(1-\gamma)$ is the molecular density inside the furnace at temperature T and with the gas plenum pressure P_p used in measuring $Q_\perp(H+H_2)$, $n_F(T_r)$ is the molecular density in the furnace at room temperature, $\overline{v_M(T)}$ and $\overline{v_M(T_r)}$ refer to mean molecular velocities inside the furnace, $\overline{v'_M(T)}$ and $\overline{v'_M(T_r)}$ refer to the mean molecular velocities in the atom beam, and γ is the estimated fractional dissociation of hydrogen at the temperature T and pressure $P_F(T)$. The factors

$$\{(1-\gamma)n_F(T)/n_F(T_r)\}\cdot\{\overline{v_M(T)}/\overline{v_M(T_r)}\}$$

allow for the temperature dependence of the effusion rate of the molecules from the furnace and the factor $\{\overline{v'_M(T_r)}/\overline{v'_M(T)}\}$ allows for the dependence of the excitation probability on molecular velocity. Since the molecular mean velocities are proportional to the square root of the furnace temperature T, the velocity ratios cancel. Defining pressure in terms of density through the ideal gas law $P_F(T)=(1+\gamma)n_F(T)kT$, eq (7) can be simplified to

$$\int S_M(T)dt=\left\{\int S_M(T_r)dt-\int S_M(T_r)_0dt\right\}\cdot\{(1-\gamma)P_F(T)T_r\}/\{(1+\gamma)P_F(T_r)T\} \qquad (8)$$

where $P_F(T)$ is the total pressure due to atoms and molecules in the furnace at temperature T.

The estimation of $P_F(T)$ from the pressure P_p in the plenum is based on a measurement of the total conductance from the rate of decay of pressure in the plenum, at the operating pressure, and calculation of the conductance of the furnace orifice from the geometry and the assumptions of ideal gas behavior. This permits a determination of the conductance of the tubulation leading to the furnace.

The estimation of γ is described in the appendix. It is based on the assumption of thermal equilibrium. It is not possible to make a conclusive statement as to the validity of the assumption, but the evidence indicates that it is useful as the basis for approximate calculations. The mean-free-path of molecular hydrogen [Dushmann, 1962] at 25 millitorr is comparable with the 2.4 mm radius of the furnace, but short compared to its length, so that an atom or molecule should be contained within the central hot section of the furnace but should make frequent wall collisions. Investigations of the interaction of hydrogen with tungsten surfaces [e.g., Hickmott, 1960] indicate that there is a substantial molecular sticking probability (~ 0.05) not very dependent on temperature, and that atomic hydrogen is evaporated from the surface at a rate consistent with equilibrium thermodynamics.

The velocity of gas flow is negligible compared to the atom velocities and therefore would not interfere with the effectiveness of wall collisions in establishing equilibrium.

Indirect evidence of approach to thermal equilibrium lies in the observation that the Lyman-α signal saturates rapidly as the temperature rises above 2000 K. Similar observations were noted by Lockwood and Everhart [1962] in connection with charge exchange between protons and hydrogen in a tungsten furnace.

The correction $C(H_2)$ to $Q_\perp(H+H_2)$ as given by eq (6) is

$$C(H_2)=\int S_M(T)dt/P'_p\left\{\int I'dt-\int I'_0dt\right\} \qquad (9)$$

where the values of the current I' and I'_0, are those registered during the measurement of

$$\left\{\int S_M(T_r)dt-\int S_M(T_r)_0dt\right\},$$

and P'_p is the average value of the plenum pressure. As in the application of eq (6) the ratios of the photon signal to electron current and plenum pressure were computed for each integration and the average of all the ratios for the same electron energy was used to calculate $C(H_2)$ for each electron energy. The cross section for production of Lyman-α radiation from hydrogen atoms alone is then

$$Q_\perp(H)=Q_\perp(H+H_2)-C(H_2). \qquad (10)$$

This procedure of subtracting two sets of relative data is only convenient if the apparatus used for the two measurements is identical (including the gains of the amplifiers), as was the case in the present work.

Since the calculation of $C(H_2)$ is not very accurate due to the uncertainties in P_F and γ and the possible effect of thermal excitation of the molecules on the cross section, the data used in calculating $Q_\perp(H+H_2)$ were taken under conditions of furnace temperature and pressure where the molecular concentration in the atomic beam was estimated to be less than 5 percent. This resulted in $C(H_2)$ being only a few percent of $Q_\perp(H+H_2)$. Since $Q_\perp(H)\cong Q_\perp(H+H_2)$, even a 100 percent error in $C(H_2)$ could not alter the value of $Q_\perp(H)$ more than 2 percent.

The energy dependence of $C(H_2)$ is, of course, the same as for a relative cross section $Q_\perp(H_2)$. From the relative values of $C(H_2)$ as given by eq (9) and of $Q_\perp(H)$ as given by eq (10), it is possible to determine the ratio of the atomic to the molecular cross sections by taking account of the relative densities of atoms and molecules in the beam at the temperature T used in eq (7). Since, as stated above, the effects of relative velocities on the relative effusion rates and on the relative beam densities of the two components cancel, the ratio of densities in the beam is the same as in the furnace and may be stated in terms of the dissociation fraction γ at temperature T, assuming thermal equilibrium as in all this discussion. The significance of the molecular cross section is rather arbitrary since it is determined by the band pass of the Lyman-α detectors.

4. Results

4.1. Threshold Data

The first investigation conducted with the apparatus described was of the threshold behavior of the Lyman-α production cross section. The results have been published [Chamberlain et al., 1964; Moiseiwitsch and Smith, 1968] and are included here in figure 5 for completeness.

Since the electron energies used in that work were less than the threshold for production of radiation in the band of sensitivity of the photon detector (1050 to 1340 Å) from H_2 molecules, which was about 1.4 eV above the Lyman-α energy of 10.2 eV, several advantages ensued:

(1) The results were independent of the degree of dissociation of the hydrogen beam. Of course, high dissociation was desired to obtain appreciable photon intensities.

(2) Over the small electron energy and consequent gun voltage ranges, there were no significant changes in the following parameters:

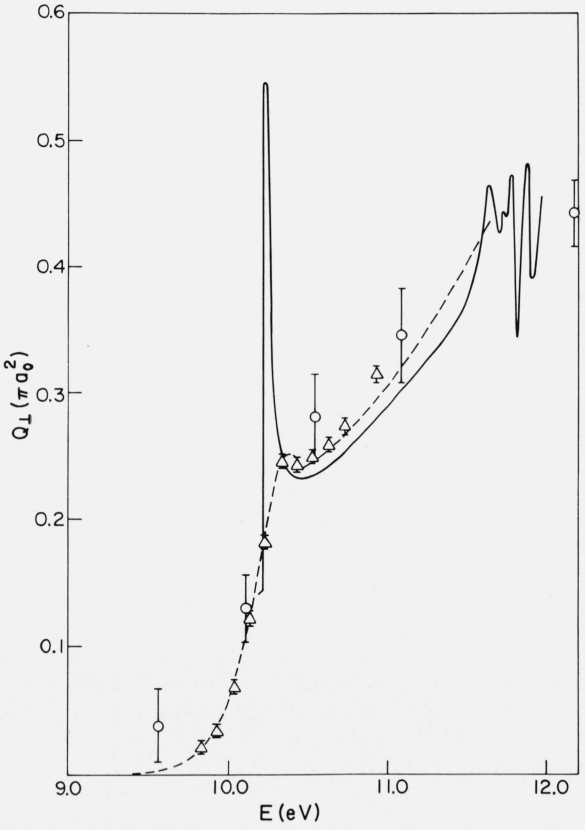

FIGURE 5. *The relative cross section for excitation of the* 2p *state of atomic hydrogen is shown as measured in this laboratory by Chamberlain, Smith and Heddle [1964], △; by Fite, Stebbings, and Brackmann [1959], ○; and as calculated by Burke, Taylor, and Ormonde [1967], solid curve.*

The dashed line results from folding the electron energy distribution used by Chamberlain *et al.* into the solid curve from Burke *et al.* This permits a valid comparison of theory and experiment. The error bars on the triangles represent the standard deviations of the mean values; those on the circles are confidence limits.

(a) Electron beam focus, and
(b) x-ray production (believed important in later work, see below).

The price for these advantages included the necessity for a narrow, well-measured electron beam energy distribution and careful measurement of any changes in the contact potential, neither being restrictive in later work. It was also necessary to use low electron current (~ 1.5 μA) so that space charge effects on current collection efficiency were negligible.

The most interesting feature of the threshold work was the plateau in $Q_\perp$ near the threshold, which is consistent with a finite value of $Q_\perp$ at threshold. In addition to the agreement with theory previously noted [Chamberlain et al., 1964] these results have been found to be in good agreement with recent calculations by Burke, Ormonde, and Whitaker [1966] and by Burke, Taylor, and Ormonde [1967], as can be seen in figure 5.

4.2. Results From Threshold to 200 eV

After completion of the threshold investigation, the emphasis was shifted to the shape of the excitation cross section at higher energies. Measurements there would permit additional comparisons with theory and previous experiments and normalization of the relative measurements to Born approximation calculations of the cross section. However, this work has been complicated by additional instrumental problems, primarily due to differing electron gun characteristics over the larger electron energy range, which have proved difficult to solve.

For electron energies greater than 90 eV, the electron gun was operated in an accelerating lens mode rather than the decelerating mode used at lower energies, as was described in section 2.4. A necessary condition for a successful measurement is that possible differences in the geometry of the electron beam in these two modes must not affect the results. Data were taken in both modes for cathode potentials of 70 to 90 V. On occasion the two sets of data were found to be quite different. After considerable investigation, the difficulty was removed by a thorough cleaning of the electron gun electrodes.

Another check on the operation of the apparatus was made by taking data with cathode potentials of 10 V (zero Lyman-α signal) and 40 V (near the peak of the excitation cross section) two or more times in the sequence of programed gun voltages. The purpose of this was to check for spurious voltage dependences of the data. The two different 10 V data points were always in agreement within their standard deviations, showing that the determination of the zero signal baseline was valid. However the 40 V data were not at first reproducible. This is illustrated in table 1, in which are listed photon signal data at 40 V taken after successively larger cathode potentials. The observed systematic decrease in the data implied that the high voltage data points were probably spuriously depressed. Additional studies showed that the magnitude of this effect decreased with time after exposure at the high voltage

data point. These effects were attributed to a short term change in the sensitivity of the ion chamber.

TABLE 1. *Effect of preceding gun voltages on the apparent relative photon intensity at 40 eV electron energy, using a LiF covered detector*

Voltage sequence	Mean value of 40 V measurements	Standard deviation of the mean value
30→ 40 V	0.0548	±0.0006
90→ 40 V	.0517	±.0004
120→ 40 V	.0507	±.0005
150→ 40 V	.0498	±.0004
200→ 40 V	.0489	±.0004

One possible cause of this phenomenon was a buildup of charge on the LiF window of the ion chamber from scattered electrons, which might change the electric field inside the ion chamber and thus the detection efficiency. Since the differential electron scattering cross section and the electron beam trajectory change with energy, this would be an energy dependent effect which would also be time dependent, owing to the finite surface resistance of the LiF window. This hypothesis was tested in two ways: a second LiF window was placed in front of the ion chamber with a grounded wire mesh in front of it (the grounded mesh on the surface of the ion chamber window itself was retained), so that scattered electrons deposited on the extra window could not make as large a change in the sensitivity of the detector, and a magnetic field of about 7 G was established parallel to the electron beam axis, in order to reduce the number of electrons that traveled perpendicular to the electron beam axis. These measures did not improve the agreement among the 40 V data, so another solution was sought.

Heath and Sacher [1966] have shown that LiF is particularly sensitive to irradiation by 1 and 2 MeV electrons, the transmittance at the Lyman-α wavelength of the sample tested decreasing from 60 percent before to 2 percent after irradiation. On the other hand the transmittance of a MgF_2 sample decreased only from 52 percent to 36 percent under the same conditions. To test the behavior of MgF_2 in the present situation an extra window of that material was placed in front of the ion chamber window (still LiF). The results were favorable: the 40 V data were in much better agreement. Therefore, the LiF window was removed from the ion chamber and a MgF_2 window installed, with the recognition of further possible advantages in the longer wavelength cutoff (1130 versus 1050 Å) and lower water absorbency of this material. Due to the need for insensitivity to the polarization of the Lyman-α radiation, a polished crystal of MgF_2 with its optical axis perpendicular to the faces of the window was used. With the window alone, all 40 V data were in agreement within their standard deviations, as expected. Therefore, although Heath and Sacher's work [1966] showed that MgF_2 was not impervious to radiation damage, it was much less affected than LiF in this application.

Since the possibility of electrons hitting the window of the detector had been discounted, we suggest that the trouble with LiF may have been caused by soft x-rays coming from parts of the electron gun electrodes exposed to the electron beam, e.g., the edges of the electron beam apertures. Although it is well known that hard x-rays affect the optical properties of LiF by production of *f*-centers, etc., no mention of sensitivity to soft x-rays was found in a brief search of the literature, so this explanation is only tentative. Due to the dependence on specific apparatus geometry that this effect would have, it is not possible to estimate its importance in other experiments. However, it may possibly have contributed to the anomalous results noted by Fite and his co-workers [Ott et al., 1967].

During the course of taking data, exceptionally large noise pulses in the photon signal occurred rather regularly. The pulses originated in the ion chamber since they did not occur when the ion chamber voltage was reduced. They were readily detected as large discontinuities in the continuously recorded output of the integrating circuit. Some may have been caused by cosmic rays (an early ion chamber design incorporated uranium glass whose radioactivity was readily detectable) but most were believed due to voltage breakdown inside the ion chamber. These events were orders of magnitude larger than the usual noise. In order to overcome these large errors, the output was monitored visually and spoiled data replaced with immediate repetitions. Spoiled data that were missed during visual monitoring were replaced by good data taken at another time the same day. These corrections were made with the aid of the graphic record of the integrator output during editing of the punched data cards.

Correction of the data by interpretation of the integrator output records has the disadvantage that bias in choosing data points for rejection is possible. The pulses occur in all phases, presumably with equal probability, and may make either positive or negative contributions to the integrated signals. Some bias is possible because the positive pulses have a different appearance in the recorded integral than do negative pulses. (Recently data rejection based on oscilloscope triggering with the discriminator set well above the random noise level has exhibited significant improvement over the edited data. Pulse rejection is phase independent. Statistical errors were significantly reduced.)

Table 2 presents the results of a run of 38 cycles. With the results are listed the standard deviations of the means of the individual data points. The consistency of the 40 V points is noteworthy, as is the agreement within pairs of 70 and 90 V points taken in the two different modes of electron beam focusing.

Table 2 also shows the results of measurements of the molecular excitation cross section required to correct $Q_\perp(H+H_2)$ using equations (9) and (10). The relative cross section $Q_\perp(H)$ corrected for molecular excitation is given in table 2, column 5. In column 6 $Q_\perp(H)$ is presented, normalized to the Born approximation [Moiseiwitsch and Smith, 1968], with an allowance of 2 percent for cascading.

TABLE 2. *Measured values of the relative cross section for electron impact excitation of hydrogen*

Nominal [a] cathode potential	Electron [b] energy	$Q_\perp(H+H_2)$ from eq (6) in text	$C(H_2)$ from eq (9)	$Q_\perp(H)$ from eq (10)	$Q_\perp(H)$ [c]
V	*eV*				(πa_0^2)
10	8.4	−0.0008±0.0013			
12.5	11.0	+.0263± .0016		0.0263	0.259±0.016
15.0	13.4	.0546± .0010	0.0001	.0545	.537± .010
17.5	16.0	.0655± .0009	.0004	.0651	.642± .009
20.0	18.5	.0715± .0010	.0007	.0708	.698± .010
25.0	23.5	.0818± .0010	.0009	.0809	.796± .010
30	28.5	.0872± .0010	.0010	.0862	.850± .010
40	38.6	.0887± .0010	.0012	.0875	.863± .010
50	48.6	.0865± .0011	.0013	.0852	.840± .011
10	8.4	+.0008± .0013			
70	68.6	.0807± .0012	0.0013	0.0794	0.783±0.012
*70	68.6	.0801± .0014	.0013	.0788	.777± .014
90	88.7	.0736± .0013	.0012	.0724	.714± .013
*90	88.7	.0749± .0013	.0012	.0737	.727± .013
40	38.6	.0878± .0014	.0012	.0866	.854± .014
*120	118.8	.0640± .0012	.0011	.0629	.620± .012
40	38.6	.0886± .0013	.0012	.0874	.862± .013
*150	148.9	.0585± .0008	.0010	.0575	.567± .008
40	38.6	.0884± .0012	.0012	.0872	.860± .012
*200	199.1	.0501± .0007	.0008	.0493	.486± .007
40	38.6	.0870± .0010	.0012	.0858	.846± .010

[a] Starred values signify the accelerating focusing mode; unstarred values the decelerating focusing mode.
[b] Corrected for contact potential and power supply nonlinearity.
[c] Normalized to the Born approximation at 200 eV.

The statistical errors in the results listed in table 2 are about 1.5 percent of the peak value at 40 eV. The significance of systematic errors is difficult to estimate. The errors associated with the electronic measurement instrumentation, consisting of carefully calibrated high quality systems, may be of the same order as the statistical error. Of more concern is the possibility of small residual errors of the type which appeared on a larger scale requiring corrective measures as has been described above: sensitivity of windows to low energy radiation, apparent charging up of surfaces, stray fields, etc. The evidence that such effects as these are not serious is largely circumstantial:

(1) The statistics show that the measurement with the automatic rejection system is very stable. Such effects as surface charging should lead to erratic performance of the apparatus.

(2) The signal at 40 V was completely independent of its position in the cycle.

(3) The 70 V and 90 V points were consistent when measured in the two focusing modes. This suggests insensitivity of the result to electron beam geometry and demonstrates that there is no serious field penetration from the anode potentials.

5. Discussion and Conclusion

In order to facilitate comparison of our relative data with data from other experiments and with theoretical calculations, they were normalized to a value for $Q_\perp(H)$ at 200 eV that was interpolated from values calculated using the Born approximation: $Q(H)=0.486\ \pi a_0^2$. This value includes a cascade contribution to the population of the $H(2p)$ state of about 2 percent. The normalized data are shown in figure 6 along with the earlier experimental data of Fite and Brackmann [1958] and Fite et al. [1959] and some theoretical cross sections. Our data are in agreement with those of Fite and his co-workers within the quoted experimental error estimates, except very near to threshold where uncertainty in absolute electron energy makes comparison difficult. The two sets of measurements were made with somewhat independent techniques since Fite and his co-workers used an iodine vapor ion chamber with a molecular oxygen filter and LiF windows whereas we used a nitric oxide ion chamber with a MgF_2 window and no filter. The smaller limits of error on our data are probably due to the lower background gas pressure in our apparatus and the automated data acquisition system that we used, which facilitated the collection of more data.

Two of the several theoretical calculations [Burke and Smith, 1962; Moiseiwitsch and Smith, 1968] of the $H(2p)$ excitation cross section are included in figure 6. The Born approximation curves [Moiseiwitsch and Smith, 1968] are included to demonstrate the validity of the normalization of the data to a value deduced from that theory at 200 eV. Note that the experimental data fall on the curve down to about 125 eV. However the Born approximation values are considerably larger than the experimental values at lower energies where the former are not expected to be valid.

The second theoretical curve plotted in figure 6 is the result of a close coupling calculation including the 1*s*, 2*s*, and 2*p* states of hydrogen [Burke et al., 1963]. Note that it, too, is quite different from the experimental curve, both in the size and the energy of the maximum value of the cross section. The disagreement in size seems even more striking when it is remembered that the experimental values include a cascade contribution and so ought to be larger than the theoretical values, which do not include cascade in that energy region.

The good agreement between the experimental measurements of the relative cross section for production of Lyman-α radiation suggests that there are no serious errors in them and that the lack of agreement with theory appears to be a fault of the latter. Thus a need for further theoretical work is indicated. Additional experimental investigations are also underway in our laboratory and elsewhere with the emphasis on measuring the angular distribution of the photons [Ott et al., 1967] and microscopic details of the cross section [Burke et al., 1966, 1967].

We acknowledge the cooperation of members of the technical staff of the Joint Institute for Laboratory Astrophysics in the design and construction of much of the apparatus and the work of G. Chamberlain and D. Heddle in obtaining the threshold data. We appreciate the assistance of John Vornhagen at Harshaw Chemical Company on our problem with the ion chamber windows.

6. Appendix: Estimation of the Dissociation Fraction, γ

Assuming thermal equilibrium applies, the degree of thermal dissociation, γ, of molecular hydrogen in the

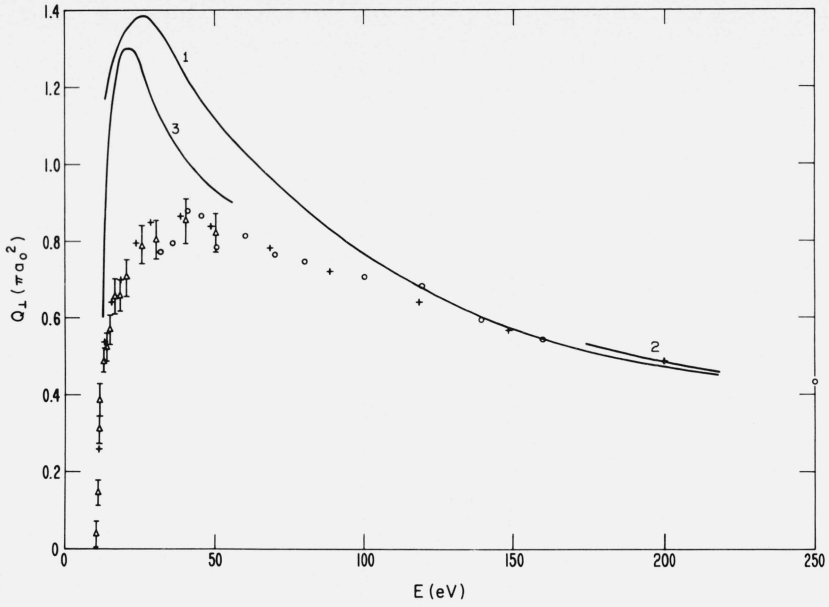

FIGURE 6. *The results of relative measurements of electron impact excitation of the* 2p *state of atomic hydrogen, from Table 2, shown as crosses* (+), *are compared with the experimental results obtained by Fite and Brackmann (1958), circles* (○); *and with the threshold results of Fite, Stebbings, and Brackmann (1959), triangles* (△).

The error bars shown on the triangles are confidence limits as are the ±12% errors assigned to the points represented as circles. Statistical probable errors associated with the present work are about 1%, but the accuracy may be limited by systematic errors two or three times larger. Curve 1 shows the Born approximation result (see Moiseiwitsch and Smith, 1968) and the experimental results are normalized to curve 2 which allows for cascading. Curve 3 is a 1s-2s-2p close coupling calculation (Burke, Schey and Smith, 1963).

tungsten furnace depends on the furnace temperature T and pressure P_F inside it according to the following relation [Wooley, 1955; Liepmann and Roshko, 1957]:

$$\gamma^2 = \frac{K(T)}{4P_F + K(T)},$$

where $K(T)$ is the dissociation constant for the reaction $H_2 \leftrightarrows 2H$ at the temperature T. Values of $K(T)$ are tabulated by Wooley [1955] and by Stull and Sinke [1956]. Wooley [1955] also presents a useful chart relating P_F, γ, and T, whereby any of the three quantities can be found from the other two.

Of the three quantities above only the furnace temperature T was measured directly. The gas pressure P_p was measured upstream from the furnace at the plenum in the gas manifold. The pressure in the furnace is related to the plenum pressure in a complicated manner depending on the conductances of various elements of the gas handling system, on the furnace and manifold temperatures, and on the degree of dissociation of the gas. If thermal equilibrium is assumed in the furnace this relation can be derived.

The following symbols will be used:

P_p = gas plenum pressure
T_r = room temperature
n_F = (number of H_2 molecules per cm^3) + (one-half the number of H atoms per cm^3)
$C_1^m(T_r)$ = conductance (cm^3/s) of the gas handling elements leading from the plenum to the furnace and assumed to be at room temperature
$C_2^m(T)$ = conductance (cm^3/s) of the furnace orifice for molecules at the temperature of the furnace
$C_2^g(T)$ = conductance (cm^3/s) of the furnace orifice for atoms at the temperature of the furnace
n_p = number of molecules in the gas plenum per cm^3.

The flow equations for molecular and atomic hydrogen are:

number of molecules per second flowing into the furnace $= C_1^m(T_r)[n_p - n_F]$;
number of molecules per second flowing out of the furnace $= C_2^m(T)[(1-\gamma)n_F]$;
number of atoms per second flowing out of the furnace $= C_2^g(T)[2\gamma n_F]$.

Conservation of mass flow is now applied by equating the mass flow rate into the furnace to the mass flow rate out of the furnace, where m_{H_2} is the mass of molecular hydrogen and m_H is the mass of atomic hydrogen.

$$m_{H_2}C_1^m(T_r)[n_p - n_F] = m_{H_2}C_2^y(T)[1-\gamma]n_F + m_H C_2^g(T)[2\gamma n_F]. \quad \text{(A1)}$$

Using the fact that $m_{H_2} = 2m_H$ and solving for n_F, eq (A1) becomes

$$n_F = n_p \left[\frac{1+[1-\gamma]C_2^y(T)+\gamma C_2^g(T)}{C_1^m(T_r)}\right]^{-1} \quad \text{(A2)}$$

If molecular flow is assumed then the conductance of the furnace orifice is proportional to $(T/M)^{1/2}$ [Dushmann, 1962] where M is the mass number. Hence

$$\sqrt{2}C_2^y(T) = C_2^g(T) \quad \text{(A3)}$$

and

$$\frac{C_2^m(T)}{C_2^m(T_r)} = \sqrt{\frac{T}{T_r}}. \quad \text{(A4)}$$

n_p and n_F are related to the pressures P_p and P_F respectively by the following relations:

$$P_p = n_p k T_r \quad \text{(A5)}$$

and

$$P_F = (1+\gamma)n_F k T, \quad \text{(A6)}$$

where the $(1+\gamma)$ appears in eq (A6) because dissociation occurs in the furnace. Substituting eqs (A3), (A4), (A5), and (A6) into eq (A2) gives

$$P_F = \frac{P_p(1+\gamma)T}{T_r + \sqrt{T_r T}[1+(\sqrt{2}-1)\gamma]C_2^m(T_r)/C_1^m(T_r)}. \quad \text{(A7)}$$

The dissociation fraction is not known initially and therefore the furnace pressure cannot be determined directly from this equation. However, an iteration procedure may be employed: An approximate value of γ is used in eq (A7) along with appropriate values of C_1 and C_2 and values of T, T_r, and P_p to obtain an approximate value of the furnace pressure. Using this value together with the known value of the furnace temperature T, the graph of Wooley [1955] may be used to obtain a more accurate value of γ. This procedure is continued until a set of values of γ, P_F, and T are obtained which are consistent with the input data for T and P_p through eq (A7).

It should be noted that the pressure versus temperature curve for a given dissociation [see Wooley, 1955] has a very steep slope such that a relatively large pressure change yields a small dissociation fraction change while a temperature change of the same relative amount as the pressure change would yield a very large dissociation fraction change. Therefore the dissociation fraction depends much more critically upon the temperature than upon the pressure in the furnace. Values of the total conductance, measured at different temperatures, varied over a range of approximately 20 percent. Therefore the furnace pressure P_F has a corresponding uncertainty, but the resulting uncertainty in γ is very much smaller.

As a typical example, let the gas manifold pressure be 100 torr, the furnace temperature be 2500 K, $C_1^m(T_r) = 16$ cm³/s, and $C_2^m(T_r) = 231$ cm³/s. Using the procedure described above, the furnace pressure was found to be 27 torr and the dissociation fraction to be 0.90. For the data reported in table 2, with a pressure P_p of 87 torr and temperature of 2570 K, the dissociation fraction was estimated to be 0.95 ± 0.01.

7. References

Beers, Y., Introduction to the Theory of Error, 2d ed., p. 30 (Addison-Wesley, Reading, 1957).

Burke, P. G., Proc. Phys. Soc. (London) **82,** 443 (1963).

Burke, P. G., Ormonde, S., and Whitaker, W., Phys. Rev. Letters **17,** 800 (1966).

Burke, P. G., Schey, H. M., and Smith, K., Phys. Rev. **129,** 1258 (1963).

Burke, P. G., and Smith, K., Rev. Mod. Phys. **34,** 458 (1962).

Burke, P. G., Taylor, A. J., and Ormonde, S., Proc. Phys. Soc. (London) **92,** 345 (1967); Erratum, J. Phys. B (Proc. Phys. Soc.), [2], (Proc. Phys. Soc.) Ser. [2], **1,** 325 (1968).

Carver, J. H., and Mitchell, P., J. Sci. Instr. **41,** 555 (1964).

Chamberlain, G. E., Smith, S. J., and Heddle, D. W. O., Phys. Rev. Letters **12,** 647 (1964).

Dushmann, S., Scientific Foundations of Vacuum Technique, 2d ed. (John Wiley & Sons, New York, 1962).

Fite, W. L., and Brackmann, R. T., Phys. Rev. **112,** 1151 (1958).

Fite, W. L., Stebbings, R. F., and Brackmann, R. T., Phys. Rev. **116,** 356 (1959).

Foote, P. D., Fairchild, C. O., and Harrison, T. R., Pyrometric Practice, National Bureau of Standards Technical Paper No. 170 (1921).

Heath, D. F., and Sacher, P. A., Appl. Optics **5,** 937 (1966).

Hickmott, T. W., J. Chem. Phys. **32,** 810 (1960).

Hils, D., Kleinpoppen, H., and Koschmieder, H., Proc. Phys. Soc. (London) **89,** 35 (1966).

Hunter, J. B., Platinum Metals Rev. **4,** 130 (1960).

Kohl, W. H., Materials and Techniques for Electron Tubes, p. 272 (Reinhold, New York, 1960).

Leder, L. B., and Simpson, J. A., Rev. Sci. Instr. **29,** 571 (1958).

Lichten, W., and Schultz, S., Phys. Rev. **116,** 1132 (1959).

Liepmann, H. W., and Roshko, A., Elements of Gasdynamics (John Wiley & Sons, New York, 1957).

Lockwood, G. J., and Everhart, E., Phys. Rev. **125,** 567 (1962).

Luders, G., Z. Naturforsch **5a,** 608 (1950).

Moiseiwitsch, B. L., and Smith, S. J., Rev. Mod. Phys. **40,** 238 (1968).

Ott, W. R., Kauppila, W. E., and Fite, W. L., Phys. Rev. Letters **19,** 1361 (1967).

Percival, I. C., and Seaton, M. J., Phil. Trans. Roy. Soc. **251,** A990 (1958).

Poland, D. E., Green, J. W., and Margrave, J. L., Corrected Optical Pyrometer Readings, National Bureau of Standards Monograph 30 (1961).

Silverman, S. M., and Lassettre, E. N., J. Chem. Phys. **44,** 2219 (1966).

Simpson, J. A., Rev. Sci. Instr. **32,** 1283 (1961).

Smith, S. J., and Branscomb, L. M., Rev. Sci. Instr. **31,** 733 (1960).

Stebbings, R. F., Fite, W. L., Hummer, D. G., and Brackmann, R. T., Phys. Rev. **124,** 2051 (1961).

Stull, D. R., and Sinke, G. C., Thermodynamic properties of the elements, in Advances in Chemistry, volume 18, 104 (American Chemical Society, Washington, D.C., 1956).

Watanabe, K., Matsunaga, F. M., and Sakai, H., Appl. Optics **6,** 391 (1967).

Williams, J. F., Curley, E. K., and McGowan, J. W., Bull. Am. Phys. Soc. **13,** 214 (1968).

Wooley, H. W., Effect of dissociation on thermodynamic properties of pure diatomic gases, National Advisory Committee for Aeronautics, Technical Note 3270 (1955).

Young, J. R., Rev. Sci. Instr. **34,** 891 (1963).

(Paper 72A5–519)